Optica Applicata, Vol. XLIII, No. 2, 2013
DOI: 10.5277/oa130212

Comparative analysis of thermal problems in GaAs- and InP-based 1.3-μm VECSELs

ADAM K. SOKÓŁ*, ROBERT P. SARZAŁA

Photonics Group, Institute of Physics, Łódź University of Technology,
ul. Wólczańska 219, 90-924 Łódź, Poland

*Corresponding author: adam.sokol@p.lodz.pl

In the present paper, thermal properties of arsenide and phosphide optically pumped vertical-external-cavity surface-emitting lasers (VECSELs) emitting the 1.3-μm radiation have been compared with the aid of the self-consistent finite-element method. Both monolithic VECSEL structures as well as VECSELs manufactured using the wafer fusing to combine phosphide layers with arsenide mirrors have been examined. The main goal of the paper is to discuss thermal VECSEL properties and to find an optimal material system characterized by the best thermal parameters enabling producing efficient VECSELs emitting radiation of the second telecom window (1.3 μm). In most cases, arsenide VECSELs have been found to exhibit lower thermal resistances than the phosphide ones. Besides, as expected, the most efficient heat-sinking has been determined for heat spreaders made of high thermal-conductivity materials. However, a final choice of an optimal VECSEL structure emitting the 1.3-μm radiation is still under question.

Keywords: vertical-external-cavity surface-emitting laser (VECSEL), semiconductor disk laser (SDL), 1.3 μm, thermal management, simulation, modelling.

1. Introduction

Optically pumped vertical-external-cavity surface-emitting lasers (VECSELs), also known as semiconductor disk lasers (SDLs), are modern semiconductor devices, which combine virtues of vertical-cavity surface-emitting lasers (VCSELs), edge-emitting lasers (EELs) and solid-state lasers [1]. Their unique properties give possibility to generate high-power radiation (from hundreds of milliwatts [2] to even 70 W [3]) with low-divergent, circularly symmetric output beams.

VECSELs with properly chosen active regions may be potentially used in a fibre-optic communication as emitters for the second telecom window (1.3 μm). Moreover, they enable doubling a frequency of emitted radiation into its visible range using nonlinear crystals placed in their external cavities. Thanks to high power and high quality of their laser beams, such a conversion can be relatively quite efficient. Therefore described lasers may be used in the multimedia technology to design mobile and cinema projectors, laser TV-sets and so on. Nowadays there are some various options

to develop VECSELs operating at 1.3 μm. Such VECSELs can be manufactured by monolithic growth of arsenide [4–7] or phosphide structures with GaInNAs or AlGaInAs quantum wells (QWs), respectively. Moreover, with the aid of the wafer fusion technique, it is possible to combine InP-based active regions with AlGaAs/GaAs distributed Bragg reflector (DBR) mirrors [8, 9], characterized by higher refractive--index contrast and better thermal properties than phosphide ones.

Unfortunately, high-power operation of optically pumped VECSELs is being hampered by thermal issues. Poor VECSEL thermal behaviour is a result of an intensive pumping, inefficient heat extraction and limited power conversion efficiency. As their pumping sources, single diode lasers or arrays emitting radiation of powers from few [2] to even hundreds of watts (up to 400 W [3, 10]) are usually used. Power conversion efficiency, understood as an output to pumping power ratio, is in turn of the order of few to tens percent (up to the highest now demonstrated value of about 50% [10]). It means that a significant part of absorbed energy is converted into heat, which leads to high temperature increases within their active regions. Therefore a proper design of both an epitaxial structure and assembly configuration is crucial for efficient VECSEL operation.

The paper is devoted to numerical modelling of thermal properties of various VECSELs operating at 1.3 μm. Calculations have been carried out with the aid of the self-consistent thermal finite-element method. Both monolithic arsenide and phosphide structures as well as wafer-fused ones with the InP-based active regions and the GaAs-based DBR mirrors have been investigated. Various VECSEL configurations have been compared and various factors influencing their thermal properties have been analyzed. The main goal of this work is to find both the material system characterized by the best anticipated thermal properties and the most efficient laser configuration, which could enable designing potentially high-power VECSELs operating in the second telecom window.

2. The laser structure

Figure 1 shows a structure of a typical VECSEL with an upper heat spreader. A semiconductor chip consisting of a multi-quantum-well active region and a DBR mirror is attached to a copper heat sink and closed in a copper submount. Operation of its high-thermal-conductivity heat spreader, bonded to the laser top surface with the aid of liquid capillarity, consists in accepting and spreading heat generated within the active region. The external cavity extends from its DBR mirror to the spherical output coupler. The active region is closed by a window confinement layer from the beam extraction side, which prevents carriers from diffusing to the semiconductor–air interface, where they could recombine nonradiatively.

Thermal phenomena have been simulated in the following VECSEL structures (*cf.* Table 1): the monolithic arsenide (A) one, the wafer-fused phosphide-arsenide (PA1, PA2) ones and the monolithic phosphide (P1a, P1b, P2a, P2b) ones. For each of above structures, calculations have been carried out for six different VECSEL

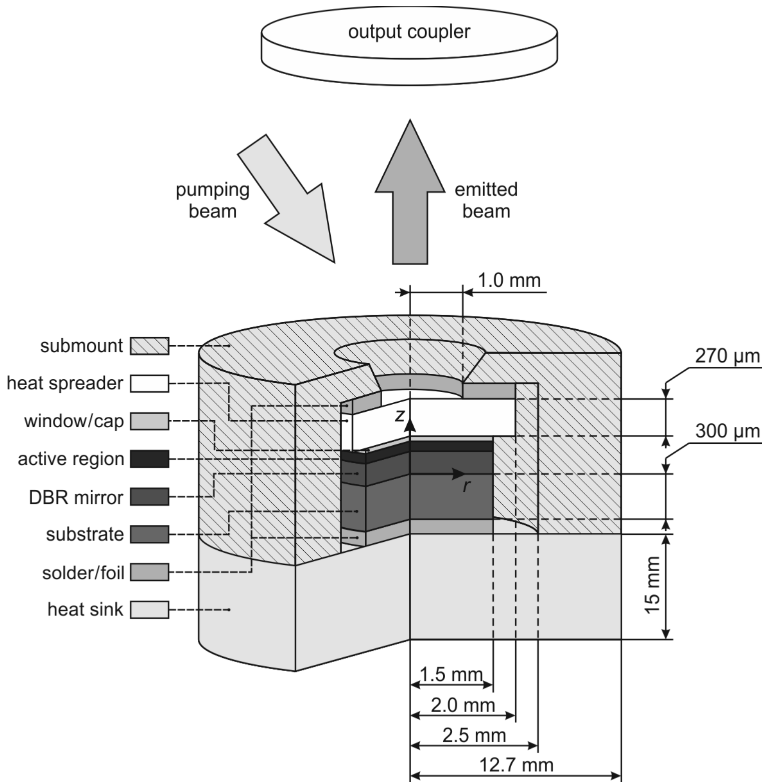

Fig. 1. Typical VECSEL structure with an upper heat spreader. Not to scale.

T a b l e 1. Modelled structures.

Structure symbol	Wavelength of pumping radiation [nm]	Active-region material (substrate)	DBR mirror material (substrate)
A	810	GaInNAs/GaAs (GaAs)	AlAs/GaAs (GaAs)
PA1	808	AlGaInAs/InP (InP)	AlAs/GaAs (GaAs)
P1a	808	AlGaInAs/InP (InP)	InGaAsP/InP (InP)
P1b	808	AlGaInAs/InP (InP)	AlGaInAs/InP (InP)
PA2	980	AlGaInAs (InP)	AlAs/GaAs (GaAs)
P2a	980	AlGaInAs (InP)	InGaAsP/InP (InP)
P2b	980	AlGaInAs (InP)	AlGaInAs/InP (InP)

configurations shown in Fig. 2. The AG configuration is assumed just to be attached to the copper heat sink. In the TD one, the substrate is completely removed. An additional internal heat spreader has been applied between the DBR mirror and the heat sink in the TDIH configuration. AGH, TDH and TDDH configurations are very similar to those of AG, TD and TDIH ones, respectively, however additionally upper heat spreaders and upper copper submounts closing their semiconductor struc-

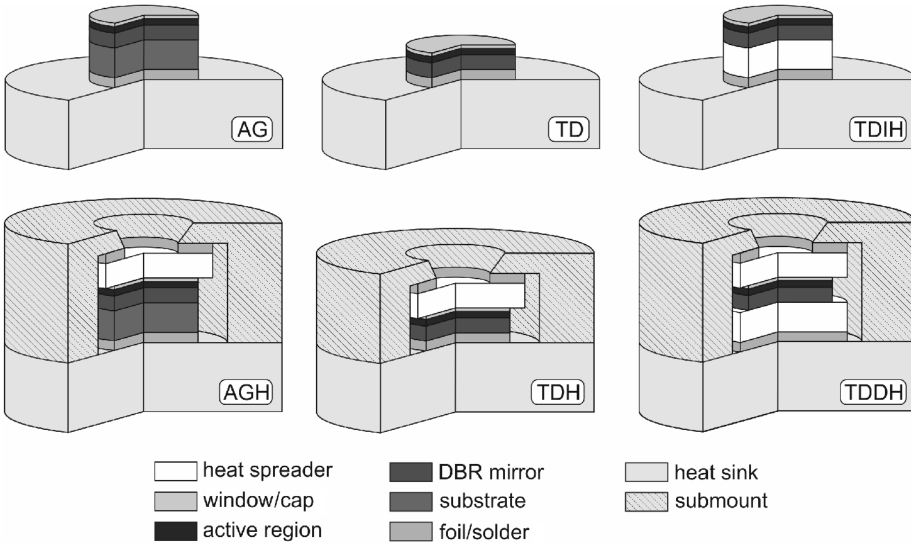

Fig. 2. Considered VECSEL assembly configurations: AG – as-grown, TD – thin device, TDIH – thin device with an internal heat spreader, AGH – as-grown with an upper heat spreader, TDH – thin device with an upper heat spreader, TDDH – thin device with a double heat spreader. Not to scale.

tures have been used. Following denotation describing specific lasers has been assumed: structure(configuration), *e.g.*, A(AGH) laser or PA1(TD) laser.

In order to make easier the comparative analysis of thermal properties of described VECSELs, following assumptions concerning their structures have been taken into account in our calculations:

– Active regions consist of five pairs of QWs separated by absorbing barriers. All pairs are located in successive antinodes of laser standing waves (resonant periodic gain configuration). Optical length of active regions is $3\lambda_{\mathrm{emit}}$ (where λ_{emit} is the wavelength of emitted radiation).

– Optical length of window layers is equal to $\lambda_{\mathrm{emit}}/2$.

– All heat spreaders are made of natural diamonds of 270 μm thickness.

– 300 μm substrate is used in the AG and AGH configurations.

– All structures are attached to the copper heat sink of 15 mm thick and 25.4 mm wide.

– VECSEL structures in the AGH, TDH and TDDH configurations are closed in copper submounts of geometrical dimensions shown in Fig. 1.

– Bottom heat sink surfaces are kept at constant temperature of 300 K.

– Number of DBR layers are chosen to achieve reflectance of the 99.9% order.

The following VECSEL structures are considered:

– The A structure, which has been designed on the basis of results published in [4–7]. According to these papers, the VECSEL structure is set on the GaAs substrate and its DBR mirror consists of 25.5 pairs of the AlAs/GaAs layers. In the active region, five pairs of the 7-nm thick $Ga_{0.63}In_{0.37}N_{0.012}As_{0.988}$ QWs are separated by the GaAs

barriers (13-nm in each pair and 158-nm between neighbouring pairs). Calculated thicknesses of outer barriers and the $Al_{0.3}Ga_{0.7}As$ window layer are 192 and 203 nm, respectively. On the top surface, the thin 1-nm cap layer has been applied to prevent from oxidation layers below. In its AGH configuration, semiconductor structures have been mounted on the heat sink with the aid of the 125-μm thick indium foil (as in [4–7]). In fact, from the point of view of thermal issues, it is practically unimportant if thick foil or thin solder is used in structures with such thick substrates. It can be seen in Fig. 3 which shows a relation between the maximal temperature T_{max} and indium layer thickness d_{In} for various configurations of A structure. Simulations have been carried out for the power of heat sources P_Q = 5 W and the pumping-beam $1/e^2$ diameter ϕ = 200 μm.

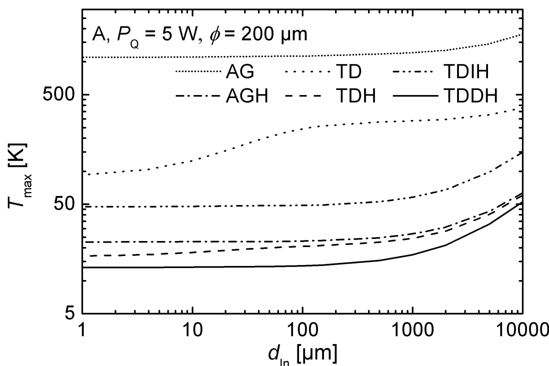

Fig. 3. Relation between the maximal temperature T_{max} and indium layer thickness d_{In} for various configurations of the A structure. P_Q is power of heat sources and ϕ is the pumping-beam $1/e^2$ diameter.

Moreover, one can see that also in the case of configurations with internal heat spreaders (TDIH, TDDH) the In-layer thickness has rather a limited influence on the device temperature in the 1–200 μm range. However, the 125-μm foil has been replaced with the 4-μm thick indium solder in these configurations, since, after such difficult and expensive technological process as substrate removing or internal heat spreader applying, it is natural to use as thin solders as possible not to decrease the device thermal properties. The 4-μm thick indium solder has been also applied in TD and TDH configurations since in these cases the thick In-foil becomes a more serious barrier for heat fluxes flowing from the active region towards the heat sink. The solder has been also used in the AG assembly to increase its thermal properties as much as possible. Described laser is pumped by a fibre-coupled laser diode array emitting the 810-nm radiation.

– The PA1 structure has been designed following the results published in [8, 9]. According to them, its structure contains the InP-based active region and the arsenide DBR mirror, which are manufactured in two separate epitaxial processes and then they are connected with each other with the aid of the wafer fusion technique. First, the active region consisting of five pairs of the 7-nm $Al_{0.14}Ga_{0.18}In_{0.68}As$ QWs

separated by the 158-nm thick InP barriers is grown on the InP substrate. Then, the active-region thickness becomes equal to $3\lambda_{emit}$. In each pair, there are additionally three 10-nm strain-compensation $Al_{0.28}Ga_{0.26}In_{0.46}As$ layers. On the active region, the 255-nm $Al_{0.53}In_{0.47}As$ window layer and the 10-nm InP cap layer are applied. Then, in the case of the structure reported in [8, 9], the DBR mirror consisting of 35 pairs of the $Al_{0.9}Ga_{0.1}As/GaAs$ layers has been deposited on the GaAs substrate. However, in order to unify modelled lasers for our comparative analysis, the same AlAs/GaAs mirror as in the A structure has been assumed in our calculations. As it has been mentioned, the InP-based active region and the arsenide DBR mirror are connected with the aid of the wafer fusion process. Then, the InP substrate is completely removed by wet etching. The complete structure is set on the copper heat sink and closed in the copper submount. The clamping of the AGH configuration has been completed by using the 125-μm indium foil, whereas in remaining arrangements, by the 4-μm indium solder. Described laser is pumped by the fibre-coupled laser diode emitting the 808-nm radiation.

– The PA2 structure has been also projected using the results published in [8, 9] and is very similar to the PA1 structure. However, in this case, the wavelength of the pumping radiation is equal to 980 nm instead of 808 nm used in the previous case. Because of that, InP barriers in the active region have to be replaced by $Al_{0.31}Ga_{0.16}In_{0.53}As$ ones of a lower bandgap. The window layer should be made of InP instead of $Al_{0.53}In_{0.47}As$ and the cap layer is not necessary, as there is no risk of oxidation. The above differences are the only ones between the PA2 and the PA1 structures.

– Monolithic phosphide P1a, P1b, P2a and P2b structures have been designed by modifying the PA1 and the PA2 structures, in which their arsenide DBR mirrors are replaced by phosphide ones. In the case of the P1a and the P2a structures, 72 pairs of the InGaAsP/InP layers have been applied, where the InGaAsP material composition is selected to have the bandgap corresponding to the 1.18-μm radiation. In the P1b and P2b structures, on the other hand, the DBR mirror has been composed of 48 pairs of the $Al_{0.2}Ga_{0.27}In_{0.53}As/InP$ layers. In order to reduce overall laser thermal resistance, all indium foils are replaced by the 6-μm aluminium ones. Both the above InGaAsP and $Al_{0.2}Ga_{0.27}In_{0.53}As$ materials have a lower bandgap than the InP one, so, in the P1a and P1b structures, phosphide DBR mirrors do not confine carriers in the active region. Therefore, to reduce carrier out-diffusion, the additional 255-nm $Al_{0.53}In_{0.47}As$ layer has to be placed between the active region and the mirror. In this way, it plays an analogous role as the upper window confinement layer.

Diagrammatic graph of band structures of materials anticipated to be used to manufacture considered lasers is shown in Fig. 4. It was developed with the aid of models and parameters described in [11] with the aid of data published in [12–16]. In the case of bulk materials (used in barriers, windows and DBR layers), strain resulting from a lattice mismatch is not taken into account. Therefore Fig. 3 may only schematically show some problems connected with carrier confinements. As an example, the band structure of the A laser is shown in Fig. 5.

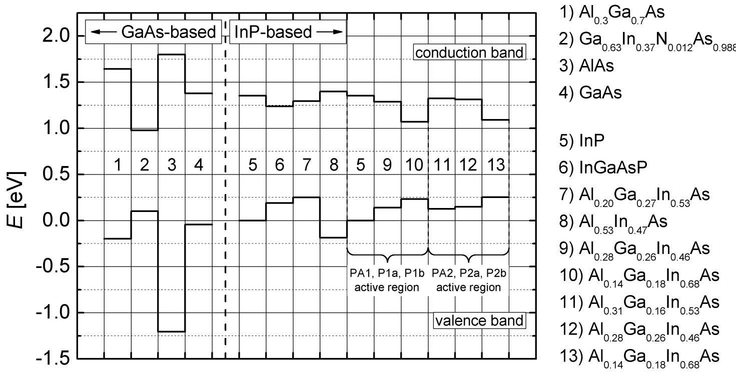

Fig. 4. Positions of the conduction and valence band edges in considered materials [11–16].

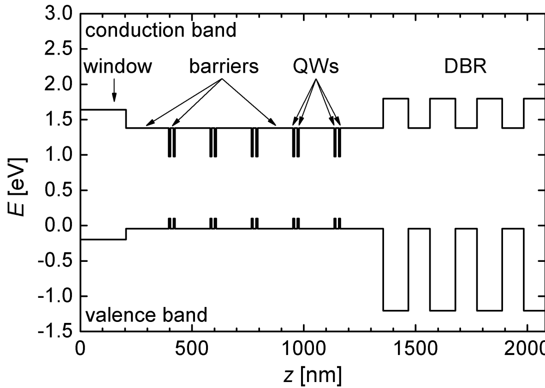

◀ Fig. 5. Band structure of the A laser.

Table 2 contains material parameters assumed in our thermal simulation, *i.e.*, thermal conductivities at 300 K ($k_{300\mathrm{K}}$) and their thermal dependences as well as absorption coefficients for the pumping radiation estimated taking into account literature data.

Due to the lack of experimental values of the absorption coefficient of AlGaInAs, it has been assumed to be the same as for InP. However, the results of our calculations show that it has rather a limited influence on device temperature. Even assuming that it is two times higher than for InP (65278 1/cm), the utmost change of the maximal temperature of modelled devices does not exceed 2% (1% on average).

The following formula describing the $\mathrm{Ga}_{1-x}\mathrm{In}_x\mathrm{N}_y\mathrm{As}_{1-y}$ thermal conductivity at 300 K has been derived on the basis of its values in the binary InN, GaN, InAs and GaAs:

$$k_{\mathrm{GaInNAs}}(x, y, 300\ \mathrm{K}) = \left[\frac{xy}{k_{\mathrm{InN}}(300\ \mathrm{K})} + \frac{(1-x)y}{k_{\mathrm{GaN}}(300\ \mathrm{K})} + \frac{x(1-y)}{k_{\mathrm{InAs}}(300\ \mathrm{K})} + \frac{(1-x)(1-y)}{k_{\mathrm{GaAs}}(300\ \mathrm{K})} + \frac{x(1-x)}{C_{\mathrm{InGaN}}} + \frac{y(1-y)}{C_{\mathrm{GaNAs}}}\right]^{-1} \quad \left[\frac{\mathrm{W}}{\mathrm{Km}}\right]$$

T a b l e 2. Material parameters assumed for thermal modelling. k_{300K} – thermal conductivity at 300 K, T – temperature, α – absorption coefficient for pumping radiation with wavelength given in brackets (∗ – assumed values).

Material	k_{300K} [W/(Km)]	$k(T)$ [W/(Km)]	α [1/cm] (λ_{pomp} [nm])
AlAs	90.9 [17, 18]	$k_{300K}\left(\frac{300\ K}{T}\right)^{1.25}$ [17, 18]	0 (810) [19]
InP	68.0 [18, 20]	$\frac{100\ W/(Km)}{1.47 + \frac{T - 300\ K}{111\ K}}$ [18, 20]	32639 (810) [21]; 599 (980) [21]; 0 (1250) [21]
GaAs	44.1 [22]	$k_{300K}\left(\frac{300\ K}{T}\right)^{1.25}$ [22]	13287 (810) [21]; 9.3 (980) [21]
$Al_{0.3}Ga_{0.7}As$	12.2 [17, 18]	$k_{300K}\left(\frac{300\ K}{T}\right)^{1.25}$ [22]	0 (810) [19]
$Ga_{0.63}In_{0.37}N_{0.012}As_{0.988}$	5.2 [18, 22–29]	$k_{300K}\left(\frac{300\ K}{T}\right)^{0.22}$ [18, 22–29]	35000 (810) [30]
$Al_{0.14}Ga_{0.18}In_{0.68}As$	4.7 [18, 31]	$k_{300K}\left(\frac{300\ K}{T}\right)^{0.36}$ [32]	32639 (810)*; 8880 (980) [33]
$Al_{0.53}In_{0.47}As$	4.5 [18, 31]	$k_{300K}\left(\frac{300\ K}{T}\right)^{1.18}$ [34]	0 (810)*
$Al_{0.31}Ga_{0.16}In_{0.53}As$	4.2 [18, 31]	$k_{300K}\left(\frac{300\ K}{T}\right)^{0.36}$ [32]	32639 (810)*; 8880 (980) [33]
InGaAsP	4.2 [18, 31]	$k_{300K}\left(\frac{300\ K}{T}\right)^{1.375}$ [35]	27700 (810) [36]; 15000 (980) [36]
$Al_{0.20}Ga_{0.27}In_{0.53}As$	4.1 [18, 31]	$k_{300K}\left(\frac{300\ K}{T}\right)^{0.36}$ [32]	32639 (810)*; 14300 (980) [33]
$Al_{0.28}Ga_{0.26}In_{0.46}As$	4.1 [18, 31]	$k_{300K}\left(\frac{300\ K}{T}\right)^{0.36}$ [32]	32639 (810)*; 8880 (980) [33]

where: $k_{InN}(300\text{ K}) = 45$ W/(Km) [23], $k_{GaN}(300\text{ K}) = 220$ W/(Km) [24], $k_{InAs}(300\text{ K}) = 26.5$ W/(Km) [18, 25], $k_{GaAs}(300\text{ K}) = 44$ W/(Km) [22], $C_{InGaN} = 1.5$ W/(Km) [24, 26, 27], $C_{GaNAs} = 1.4$ W/(Km) [28, 29]. Taking advantage of temperature dependences of thermal conductivities for the GaAs, InAs and GaN binary compounds, the following equation describing analogous temperature dependence of the GaInNAs thermal conductivity within the 300–450 K may be written:

$$k_{\mathrm{GaInNAs}}(T) = k_{\mathrm{GaInNAs}}(x, y, 300\text{ K})\left(\frac{300\text{ K}}{T}\right)^{0.22} \qquad \left[\frac{\mathrm{W}}{\mathrm{Km}}\right]$$

3. Results

Thermal simulations have been carried out within the area of the considered VECSEL structures with the aid of the self-consistent thermal finite-element method. Side and top device walls have been assumed to be thermally isolated since the thermal radiation and the acceptance of thermal energy by air particles from these walls have been found to be negligible as compared with an intense heat-flux extraction by the laser copper heat sink [37]. On the other hand, the bottom surface of the heat sink is assumed to be kept at constant temperature $T_{hs} = 300$ K. In our simulations, the Gaussian intensity profile of a pumping beam and its vertical penetration through successive laser layers have been assumed. Power densities of heat generation have been determined taking advantage of absorption coefficients listed in Tab. 2.

Table 3 contains the thermal resistances of individual laser components, calculated for the modelled lasers, *i.e.*, its window layers, active region, DBR mirror and substrate. As one can see, the monolithic phosphide P1a, P1b, P2a and P2b structures are placed on the substrates of higher thermal conductivity than those of other lasers, however thermal resistances of phosphide mirrors are several times higher than those of arsenide ones. The active region of the A structure has the highest thermal conductivity amongst all investigated lasers. On the opposite, the PA2, P2a, and P2b structures pumped by the 980-nm radiation exhibit the lowest active-region thermal conductivity, however they contain low-resistive window layers. One can say, that according to Tab. 3, the A structure is probably characterized by the best thermal properties among all considered lasers, but it should be noticed that its thermal resistance depends strongly on a type of the assembly configuration.

T a b l e 3. Relative thermal resistances of individual components of modelled structures.

		Structure						
		A	PA1	P1a	P1b	PA2	P2a	P2b
Component	Window	5.5	18.7	18.7	18.7	1	1	1
	Active region	1	1.7	1.7	1.7	7.0	7.0	7.0
	DBR	1	1	20.4	13.5	1	20.4	13.5
	Substrate	1.5	1.5	1	1	1.5	1	1

Figures 6 and 7 present thermal resistances R_{th} of considered structures in their various configurations for specified pumping conditions (P_Q – power of heat sources, ϕ – pumping beam $1/e^2$ diameter). Thermal resistance R_{th} is defined as the ratio of the maximal temperature increase (as compared with the temperature $T_{\mathrm{hs}} = 300$ K of the bottom surface of the heat sink) within the laser volume $\Delta T_{\max}$ to the power of all heat sources P_Q: $R_{\mathrm{th}} = \Delta T_{\max}/P_Q$. The whole energy of the pumping radiation absorbed within the laser structure is assumed to be converted into heat. Therefore Figs. 6 and 7 enable determination of the maximal temperature within the laser volumes in a quick and simple way, *e.g.*, the thermal resistance of the A(AGH) structure for $P_Q = 5$ W and $\phi = 200$ μm is 4.6 K/W, so its maximal temperature is equal to 300 K + $P_Q \cdot R_{\mathrm{th}}$ = 323 K.

Figures 6 and 7 show that in all VECSEL configurations (except the AG one), the A structure is characterized by the lowest thermal resistance thanks to its high-conductive both the DBR mirror and the GaAs barriers in the active region. Wafer-fused PA1 and PA2 structures exhibit higher (by 15–80%) thermal resistances than the A one, especially in configurations with upper heat spreaders. In the case of the PA1 structure, it is a result of its active region of lower thermal conductivity. In spite of the InP barriers, it contains many high-resistive AlGaInAs layers (QWs and strain-compensation ones). In the PA2 structure, the active region has even higher thermal resistance due to AlGaInAs barriers. On the other hand, InP window layer significantly improves in this case the efficiency of heat extraction by the upper heat spreader. Monolithic phosphide P1a, P1b, P2a and P2b structures are characterized by even worst thermal

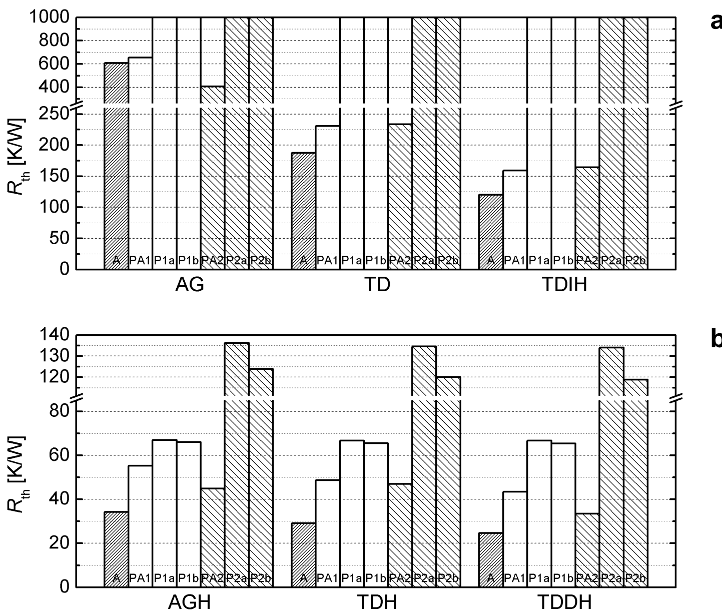

Fig. 6. Thermal resistance R_{th} of investigated structures of various assembly configurations: AG, TD, TDIH (**a**) and AGH, TDH, TDDH (**b**). $P_Q = 1$ W and $\phi = 50$ μm.

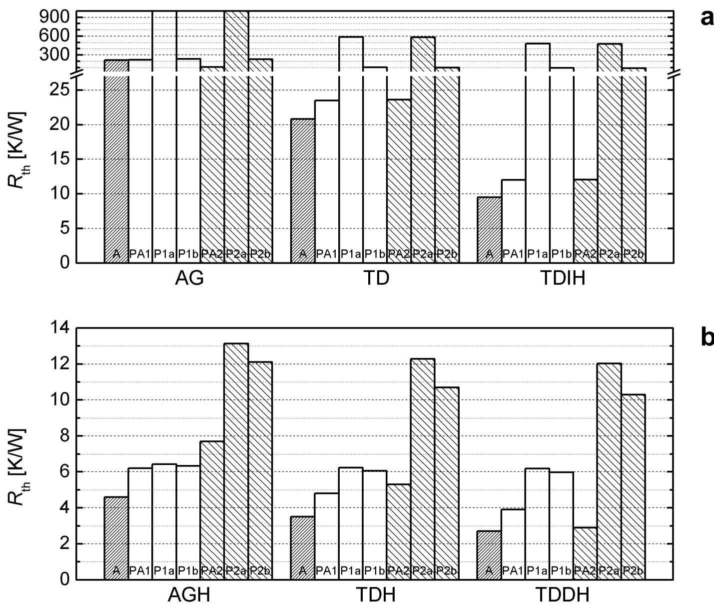

Fig. 7. Thermal resistance R_{th} of investigated structures of various assembly configurations: AG, TD, TDIH (**a**) and AGH, TDH, TDDH (**b**). P_Q = 5 W and ϕ = 200 µm.

properties (their thermal resistances are several times higher than that of the A laser), which results from low-conductive DBR mirrors.

However, one can see that structures with the AlGaInAs/InP mirrors have lower thermal resistances than structures with the InGaAsP/InP ones (in the AG, TD, TDIH configurations by 70–80% and in the AGH, TDH, TDDH ones by 1–10%), although AlGaInAs alloy is a bit more resistive. Nevertheless, the AlGaInAs/InP mirror contains only 48 pairs of semiconductor layers in comparison with 72 pairs of the InGaAsP/InP one. Therefore its overall thermal resistance is much lower (see Table 3), so heat extraction by the heat sink is more effective. However, arsenide AlAs/GaAs DBR mirrors show decidedly the best thermal properties: their thermal resistances are several times lower than those of the InP-based ones. Therefore, combining conventional phosphide active regions and high-conductive arsenide mirrors may be a good way to go around some thermal restrictions occurring in monolithic InP-based structures and may lead to designing of high-power VECSELs operating at 1.3 µm.

One can see that, depending on assembly configurations and pumping-beam parameters, the PA2 structure may have higher or lower thermal resistance than that of the PA1 one. For example, in the case of P_Q = 1 W and ϕ = 50 µm for the TD and TDIH configurations, lower temperature increases are observed for the PA1 structure (by 1–3%), whereas for other mounting structures maximal temperature within their volumes is higher by 3–30% than that in the PA2 one. For P_Q = 5 W and ϕ = 200 µm, the PA2 structure exhibits much lower thermal resistance than that of the PA1 one in

the AG (by 50%) and the TDDH (by 25%) configurations. However, for other arrangements, this quantity is higher by 0–20%.

For all considered structures, except the PA2 one, assembly configurations can be arranged from the lowest to the most efficient ones in the following order: AG, TD, TDIH, AGH, TDH, TDDH. In the case of the PA2 structure, on the other hand, substrate removal in the AG assembly for P_Q = 1 W and ϕ = 50 μm leads to a temperature increase (which is obviously not a typical situation), because it leads to a reduction of a distance between heat sources and the heat sink. Special thermal properties of the PA2 structure follow mostly from the very small absorption coefficient of GaAs for the pumping radiation (see Table 2), therefore the substrate and the DBR mirror are almost transparent for the pumping beam. It means that radiation leaving the active region is not absorbed before the solder or foil layer. In this way, there are two areas of higher temperature increases separated by the substrate. It is clear from Figs. 8 and 9 which show isotherms calculated for the PA2 structure in the AGH configuration. Moreover, Figs. 10 and 11 present axial temperature pro-

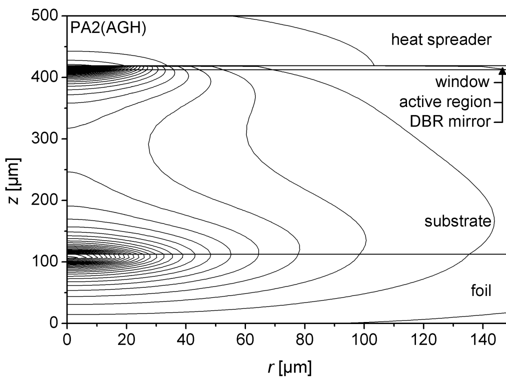

Fig. 8. Isotherms calculated for the PA2 structure in the AGH configuration for P_Q = 1 W and ϕ = 50 μm.

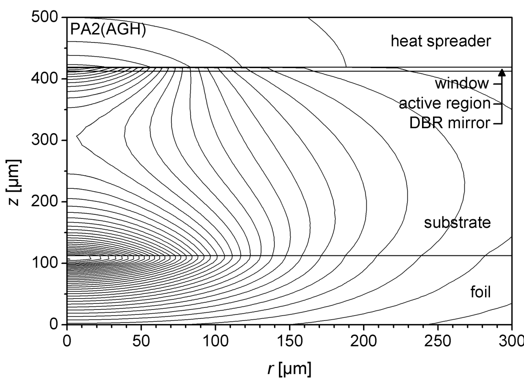

Fig. 9. Isotherms calculated for the PA2 structure in the AGH configuration for P_Q = 5 W and ϕ = 200 μm.

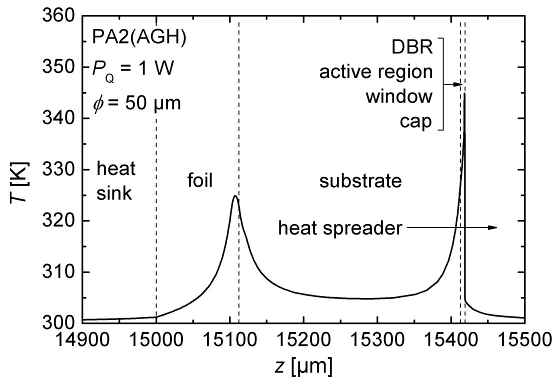

Fig. 10. Axial temperature distribution within the PA2 structure in the AGH configuration for $P_Q = 1$ W and $\phi = 50$ µm.

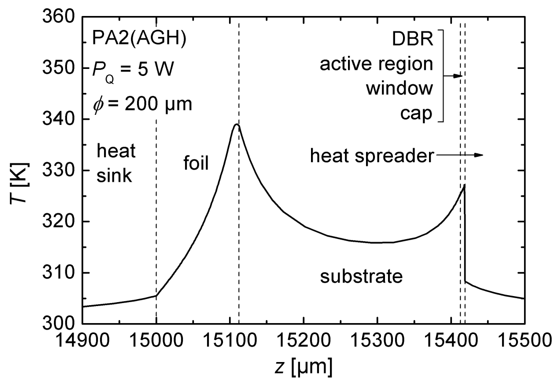

Fig. 11. Axial temperature distribution within the PA2 structure in the AGH configuration for $P_Q = 5$ W and $\phi = 200$ µm.

files within this laser. Temperature increase within the solder/foil layer is a strong barrier for the axial heat-flux flow towards the heat sink. Therefore heat flux coming from the active region has to spread in radial direction to go around this thermal obstacle. It leads to an increase in the heat-flow cross-section and is followed by more efficient heat extraction. Figure 11 shows that, for $P_Q = 5$ W and $\phi = 200$ µm, temperature increase in the solder/foil layer is higher than that in the active region. It is connected with a wide pumping-beam diameter. Then, heat generated in the active region may be extracted by the upper heat spreader through significantly larger area. It causes a considerable drop of temperature increase in this component and leads to the situation presented in Fig. 11.

Figure 12 shows a relation between the maximal temperature within the PA2 structure in the AGH configuration and the substrate thickness d_{sub} for specified pumping-beam diameters at $P_Q = 1$ W. One can see that, for narrower beams ($\phi < 100$ µm), reduction of d_{sub} leads to a temperature increase. It means that in this

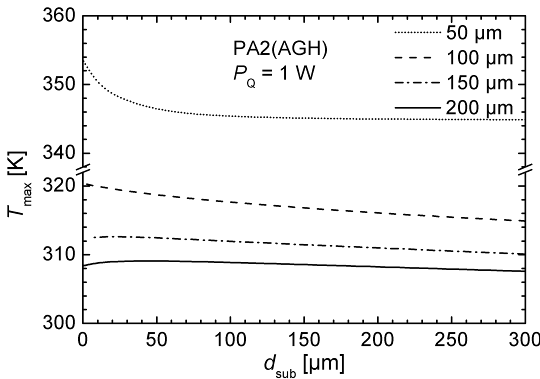

Fig. 12. The maximal temperature T_{max} within the PA2 structure in the AGH configuration versus the substrate thickness d_{sub} for various diameters of the pumping beam of the P_Q = 1 W power.

case forced heat spreading within the substrate is very strong. For wider pumping beams, curves in Fig. 11 are not monotonic and there are some maxima for d_{sub} lower than 300 μm. It is interesting to note that even a complete removal of the 300-μm substrate also leads to a temperature increase for higher diameters of the pumping beam. Therefore for ϕ = 200 μm, the TDH configuration should be characterized by higher thermal resistance than that of the AGH one. However, it has to be noted that in the first case clamping has been realized by using much thinner indium solder than in the second case, so heat extraction by the heat sink is then more efficient.

To sum up, one can say that for pumping beams wider than 100 μm, forced heat-flux spreading caused by a temperature increase in the foil layer is not crucial. Diameter ϕ = 100 μm is quite characteristic as for this value maximal temperatures within both the active region and the foil layer are equal to each other. For narrower beams, temperature increase in the active region is higher, for wider beams – lower. It means that the nature of heat flow is changing, which strongly influences laser thermal properties.

4. Conclusions

Generally, from among all considered VECSELs operating at 1.3 μm, the structure with the GaInNAs/GaAs active region exhibits the best thermal properties. Monolithic phosphide lasers show much higher thermal resistances because of high thermal resistances of the InGaAsP/InP or AlGaInAs/InP DBR mirrors. Therefore it would be an interesting idea to combine the InP-based active region with arsenide mirrors with the aid of the wafer fusion technique. Such structures are characterized by lower thermal resistances and can compete in this regard with arsenide structures. However, the whole absorbed pumping energy is assumed in our calculations to be converted into heat. In reality some part of this energy covers useful losses and is emitted as an output beam. In the case of considered structures, the power conversion efficiency

(understood as the ratio of an emitted power to an incident pumping power) for 2% output coupler and the heat-sink temperature T_{hs} = 15 °C is limited to 6% in the A structure [4–7] while to 7% and to 9% in the PA1 and the PA2 structures [8, 9], respectively. One can see that differences between these values are quite small. Therefore plots presented here may be used for a comparative analysis of considered lasers because they depend on powers of heat sources – not on incident power. In this way, there is no need to take additionally into account the pumping-beam reflection at laser top surface.

The most efficient heat removal is provided by the configurations with the upper heat-flux spreader (AGH, TDH and TDDH ones). In the case of structures with low-conductive DBR mirrors (P1a, P1b, P2a and P2b ones), differences in thermal resistances for the above mentioned configurations do not exceed 17% (as compared with that of the AGH one). For structures with arsenide DBR mirrors, substrate removal in configurations with the upper heat spreader may lead to maximal temperature reduction by 10–30% and additional application of the internal heat-flux spreader – by another 10–30%. The only exception is the PA2 structure where the low-absorbing substrate is the reason of specific laser properties, especially for narrower pumping beams. However, since an application of the upper heat spreader is usually sufficient to enable proper VECSEL operation, substrate removal or use of the internal heat spreader are often unnecessary. In the case of structures with low-absorbing substrates and DBR mirrors (*e.g*., the PA2 one), additionally forced heat-flux spreading takes place, especially for narrow pumping beams. This effect leads to reduction of laser thermal resistance to such an extent that substrate removal may lead to an unexpected temperature increase.

Acknowledgments – This work was partially supported by the COST Action MP0805 *Novel Gain Materials and Devices Based on III–V–N Compounds*.

References

[1] KUZNETSOV M., *Semiconductor Disk Lasers: Physics and Technology*, [Ed.] Okhotnikov O.G., Wiley-VCH Verlag, Weinheim, 2010, pp. 1–71.

[2] KUZNETSOV M., HAKIMI F., SPRAGUE R., MOORADIAN A., *High-power (>0.5-W CW) diode-pumped vertical-external-cavity surface-emitting semiconductor lasers with circular TEM_{00} beams*, IEEE Photonics Technology Letters **9**(8), 1997, pp. 1063–1065.

[3] CHERNIKOV A., HERRMANN J., KOCH M., KUNERT B., STOLZ W., CHATTERJEE S., KOCH S.W., WANG T.L., KANEDA Y., YARBOROUGH J.M., HADER J., MOLONEY J.V., *Heat management in high--power vertical-external-cavity surface-emitting lasers*, IEEE Journal of Selected Topics in Quantum Electronics **17**(6), 2011, pp. 1772–1778.

[4] HOPKINS J.-M., SMITH S.A., JEON C.W., SUN H.D., BURNS D., CALVEZ S., DAWSON M.D., JOUHTI T., PESSA M., *0.6 W CW GaInNAs vertical external-cavity surface emitting laser operating at 1.32 μm*, Electronics Letters **40**(1), 2004, pp. 30–31.

[5] SMITH S.A., HOPKINS J.-M., SUN H.D., BURNS D., CALVEZ S., DAWSON M.D., JOUHTI T., KONTTINEN J., *A 0.6 W CW GaInNAs vertical external-cavity surface-emitting laser operating at 1.32 μm*, Proceedings of the Conference on Lasers and Electro-Optics (CLEO), May 16–21, 2004, San Francisco, California, USA, Optical Society of America, Technical Digest (CD), paper CTuC5.

[6] CALVEZ S., HOPKINS J.-M., SMITH S.A., CLARK A.H., MACALUSO R., SUN H.D., DAWSON M.D., JOUHTI T., PESSA M., GUNDOGDU K., HALL K.C., BOGGESS T.F., *GaInNAs/GaAs Bragg-mirror-based structures for novel 1.3 μm device applications*, Journal of Crystal Growth **268**(3–6), 2004, pp. 457–465.

[7] SMITH S.A., HOPKINS J.-M., HASTIE J.E., BURNS D., CALVEZ S., DAWSON M.D., JOUHTI T., KONTINNEN J., PESSA M., *Diamond-microchip GaInNAs vertical external-cavity surface-emitting laser operating CW at 1315 nm*, Electronics Letters **40**(15), 2004, pp. 935–936.

[8] LYYTIKÄINEN J., RAUTIAINEN J., TOIKKANEN L., SIRBU A., MEREUTA A., CALIMAN A., KAPON E., OKHOTNIKOV O.G., *1.3-μm optically-pumped semiconductor disk laser by wafer fusion*, Optics Express **17**(11), 2009, pp. 9047–9052.

[9] SIRBU A., VOLET N., MEREUTA A., LYYTIKÄINEN J., RAUTIAINEN J., OKHOTNIKOV O., WALCZAK J., WASIAK M., CZYSZANOWSKI T., CALIMAN A., ZHU Q., IAKOVLEV V., KAPON E., *Wafer-fused optically pumped VECSELs emitting in the 1310-nm and 1550-nm wavebands*, Advances in Optical Technologies Vol. 2011, 2011, article 209093.

[10] CHILLA J., QI-ZE SHU, HAILONG ZHOU, WEISS E., REED M., SPINELLI L., *Recent advances in optically pumped semiconductor lasers*, Proceedings of SPIE **6451**, 2007, article 645109.

[11] SARZAŁA R.P., PISKORSKI Ł., SZCZERBIAK P., KUDRAWIEC R., NAKWASKI W., *An attempt to design long-wavelength (> 2 μm) InP-based GaInNAs diode lasers*, Applied Physics A **108**(3), 2012, pp. 521–528.

[12] GLISSON T.H., HAUSER J.R., LITTLEJOHN M.A., WILLIAMS C.K., *Energy bandgap and lattice constant contours of III–V quaternary alloys*, Journal of Electronic Materials **7**(1), 1978, pp. 1–16.

[13] VURGAFTMAN I., MEYER J.R., RAM-MOHAN L.R., *Band parameters for III–V compound semiconductors and their alloys*, Journal of Applied Physics **89**(11), 2001, pp. 5815–5875.

[14] VURGAFTMAN I., MEYER J.R., *Band parameters for nitrogen-containing semiconductors*, Journal of Applied Physics **94**(6), 2003, pp. 3675–3696.

[15] KUDRAWIEC R., *Alloying of GaN_xAs_{1-x} with InN_xAs_{1-x}: A simple formula for the band gap parametrization of $Ga_{1-y}In_yN_xAs_{1-x}$ alloys*, Journal of Applied Physics **101**(2), 2007, article 023522.

[16] ADACHI S., *Properties of Semiconductor Alloys: Group-IV, III–V and II–VI Semiconductors*, 1st Edition, John Wiley & Sons, Chichester, 2009.

[17] ADACHI S., *GaAs, AlAs, and $Al_xGa_{1-x}As$: Material parameters for use in research and device applications*, Journal of Applied Physics **58**(3), 1985, pp. R1–R29.

[18] NAKWASKI W., *Thermal conductivity of binary, ternary, and quaternary III–V compounds*, Journal of Applied Physics **64**(1), 1988, pp. 159–166.

[19] MONEMAR B., SHIH K.K., PETTIT G.D., *Some optical properties of the $Al_xGa_{1-x}As$ alloys system*, Journal of Applied Physics **47**(6), 1976, pp. 2604–2613.

[20] KUDMAN I., STEIGMEIER E.F., *Thermal conductivity and Seebeck coeffcient of InP*, Physical Review **133**(6A), 1964, pp. A1665–A1667.

[21] SOPRA N&K Database, http://refractiveindex.info; access date: November 28, 2011.

[22] AMITH A., KUDMAN I., STEIGMEIER E.F., *Electron and phonon scattering in GaAs at high temperatures*, Physical Review **138**(4A), 1965, A1270–A1276.

[23] KRUKOWSKI S., WITEK A., ADAMCZYK J., JUN J., BOCKOWSKI M., GRZEGORY I., LUCZNIK B., NOWAK G., WRÓBLEWSKI M., PRESZ A., GIERLOTKA S., STELMACH S., PALOSZ B., POROWSKI S., ZINN P., *Thermal properties of indium nitride*, Journal of Physics and Chemistry of Solids **59**(3), 1998, pp. 289–295.

[24] VITANOV S., *Simulation of High Electron Mobility Transistors*, PhD Dissertation, Technischen Universität Wien, Wien, 2010.

[25] STEIGMEIER E.F., KUDMAN I., *Thermal conductivity of III–V compounds at high temperatures*, Physical Review **132**(2), 1963, pp. 508–512.

[26] ADACHI S., *Lattice thermal conductivity of group-IV and III–V semiconductor alloys*, Journal of Applied Physics **102**(6), 2007, article 063502.

[27] PANTHA B.N., DAHAL R., LI J., LIN J.Y., JIANG H.X., POMRENKE G., *Thermoelectric properties of $In_xGa_{1-x}N$ alloys*, Applied Physics Letters **92**(4), 2008, article 042112.

[28] PALANKOVSKI V., SCHULTHEIS R., SELBERHERR S., *Simulation of power heterojunction bipolar transistors on gallium arsenide*, IEEE Transactions on Electron Devices **48**(6), 2001, pp. 1264–1269.

[29] YIMIN ZHAO, CHEN G., SHANZHONG WANG, SOON FATT YOON, *Thermal characterization of GaAsN thin films by pulsed photothermal reflectance technique*, International Journal of Nanoscience **3**(6), 2004, pp. 781–787.

[30] MIYAMOTO T., TAKEUCHI K., KAGEYAMA T., KOYAMA F., IGA K., *Chemical beam epitaxy of GaInNAs/GaAs quantum wells and its optical absorption property*, Journal of Crystal Growth **197**(1–2), 1999, pp. 67–72.

[31] GUDEN M., PIPREK J., *Material parameters of quaternary III–V semiconductors for multilayer mirrors at 1.55 μm wavelength*, Modelling and Simulation in Materials Science and Engineering **4**(4), 1996, pp. 349–357.

[32] GEHONG ZENG, JE-HYEONG BAHK, BOWERS J.E., ZIDE J.M.O., GOSSARD A.C., ZHIXI BIAN, SINGH R., SHAKOURI A., WOOCHUL KIM, SINGER S.L., MAJUMDAR A., *ErAs:*$(InGaAs)_{1-x}(InAlAs)_x$ *alloy power generator modules*, Applied Physics Letters **91**(26), 2007, article 263510.

[33] MASU K., MISHIMA T., HIROI S., KONAGAI M., TAKAHASHI K., *Preparation of* $(Al_xGa_{1-x})_yIn_{1-y}As$ $(0 \le x \le 0.5, y = 0.47)$ *lattice matched to InP substrates by molecular beam epitaxy*, Journal of Applied Physics **53**(11), 1982, pp. 7558–7560.

[34] CHENG ZHU, YONG-GANG ZHANG, AI-ZHEN LI, ZHAO-BING TIAN, *Analysis of key parameters affecting the thermal behavior and performance of quantum cascade lasers*, Journal of Applied Physics **100**(5), 2006, article 053105.

[35] ADACHI S., *Physical Properties of III–V Semiconductor Compounds*, 1st Edition, John Wiley and Sons, New York, 1992.

[36] BURKHARD H., DINGES H.W., KUPHAL E., *Optical properties of* $In_{1-x}GaxP_{1-y}As_y$*, InP, GaAs, and GaP determined by ellipsometry*, Journal of Applied Physics **53**(1), 1982, pp. 655–662.

[37] SOKÓŁ A.K., SARZAŁA R.P., *Thermal management of GaInNAs/GaAs VECSELs*, Opto-Electronics Review **21**(2), 2013, pp. 191–198.

Received June 8, 2012
in revised form September 20, 2012